# Conformational Stability and Membrane Interaction of the Full-Length Ectodomain of HIV-1 gp41: Implication for Mode of Action[†]

Naama Lev,[‡,§] Yael Fridmann-Sirkis,[‡,§] Lior Blank,[‡,§] Arkady Bitler,[||] Raquel F. Epand,[⊥] Richard M. Epand,[⊥] and Yechiel Shai*[,‡]

*Department of Biological Chemistry and Department of Chemical Research Support, The Weizmann Institute of Science, Rehovot, 76100 Israel, and Department of Biochemistry and Biomedical Sciences, McMaster University, L8N 3Z5 Hamilton, Canada*

*Received December 9, 2008; Revised Manuscript Received February 8, 2009*

ABSTRACT: Membrane fusion between the human immunodeficiency virus (HIV) and the target cell plasma membrane is correlated with conformational changes in the HIV gp41 glycoprotein, which include an early exposed conformation (prehairpin) and a late low energy six helix bundle (SHB) conformation also termed hairpin. Peptides resembling regions from the exposed prehairpin have been previously studied for their interaction with membranes. Here we report on the expression, purification, SHB stability, and membrane interaction of the full-length ectodomain of the HIV gp41 and its two deletion mutants, all in their SHB-folded state. The interaction of the proteins with zwitterionic and negatively charged membranes was examined by using various biophysical methods including circular dichroism spectroscopy, differential scanning calorimetry, lipid mixing of large unilamellar vesicles, and atomic force microscopy (AFM). All experiments were done in an acidic environment in which the protein remains in its soluble trimeric state. The data reveal that all three proteins fold into a stable coiled-coil core in aqueous solution and retain a stable helical fold with reduced coiled-coil characteristics in a zwitterionic and negatively charged membrane mimetic environment. Furthermore, in contrast with the extended exposed N-terminal domain, the folded gp41 ectodomain does not induce lipid mixing of zwitterionic membranes. However, it disrupts and induces lipid mixing of negatively charged phospholipid membranes (~100-fold more effective than fusion peptide alone), which are known to be expressed more in HIV-1-infected T cells or macrophages. The results support the emerging model in which one of the roles of gp41 folding into the SHB conformation is to slow down membrane disruption effects induced by early exposed gp41. However, it can further affect membrane morphology once exposed to negatively charged membranes during late stages.

The initial step of viral infection is mediated by viral envelope proteins (*1*). In the case of the human immunodeficiency virus (HIV)[1], the envelope protein forms a trimer, with each monomer consisting of two noncovalently associated subunits: a surface subunit gp120 and a transmembrane subunit gp41. Gp41 and gp120 are proteolytic products of the gp160 precursor (*2*). Gp41 is comprised of three functional domains: a cytoplasmic domain, a transmembrane domain, and an ectodomain, which is the most conserved region of gp41. The ectodomain contains four major functional regions: closest to the viral membrane is a Trp-rich pretransmembrane domain (PTD), followed by a C-terminal heptad repeat (CHR), an N-terminal heptad repeat (NHR), and a stretch of 15 hydrophobic residues, located at the N-terminus and termed the fusion peptide (FP) (*2*−*4*) (Figure 1).

Gp120 binds to a CD4 receptor in the target membrane and undergoes conformational changes that allow it to interact with a chemokine receptor, the coreceptor on the target membrane (*5*). These interactions trigger a cascade of conformational changes in gp120 and gp41 that result in fusion induction of the viral envelope with the target membrane, thereby initiating infection (*6, 7*). As a consequence of the conformational changes, the N-terminus of gp41 becomes exposed and interacts with the target cell membrane. This creates a prehairpin intermediate (PHI) that bridges both viral and cellular membranes (*2, 8*). The PHI is characterized by exposed NHR and CHR regions, is short-lived, and collapses after up to 30 min into a low-energy conformation of six helix bundle (SHB) (*9, 10*). In the SHB conformation, the α-helical CHR regions are packed into

* To whom correspondence should be addressed. Tel: 972-8-9342711. Fax: 972-8-9344112. E-mail: yechiel.shai@weizmann.ac.il.

[†] This study was supported by the Israel Science Foundation and by MOP 86608 from the Canadian Institutes of Health Research.

[‡] Department of Biological Chemistry, The Weizmann Institute of Science.

[§] These authors equally contributed to the study.

[||] Department of Chemical Research Support, The Weizmann Institute of Science.

[⊥] McMaster University.

[1] Abbreviations: FP, fusion peptide; CD, circular dichroism; AFM, atomic force microscopy; DSC, differential scanning calorimetry; LUV, large unilamellar vesicle; SHB, six helix bundle; LPC, 1-palmitoyl lysophosphatidylcholine; LPS, 1-palmitoyl lysophosphatidylserine; HIV, human immunodeficiency virus; PTD, pretransmembrane domain; CHR, C-terminal heptad repeat; NHR, N-terminal heptad repeat; PHI, prehairpin intermediate; IPTG, isopropyl β-D-1-thiogalactopyranoside; Rho-PE, *N*-(lissamine rhodamine B sulfonyl) dioleoylphosphatidylethanolamine; NBD-PE, *N*-(7-nitrobenz-2-oxa-1,3-diazol-4-yl) dioleophosphatidylethanolamine; PC, phosphatidylcholine; PS, phosphatidylserine.

10.1021/bi802243j CCC: $40.75 
Published on Web 02/10/2009

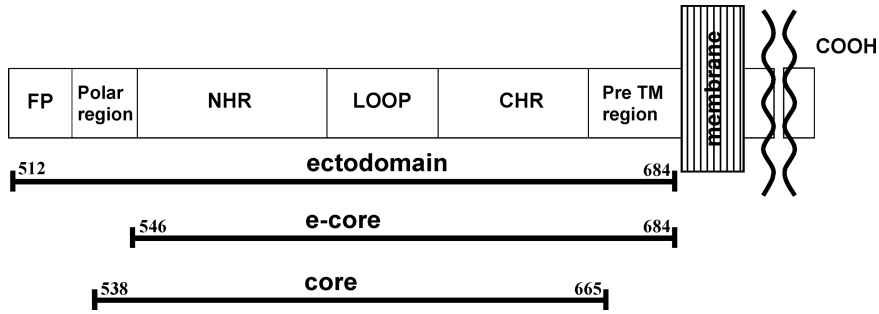


FIGURE 1: Cartoon of the HIV primary structure showing the structural and functional regions as well as their relative lengths. Below the scheme are displayed the proteins that were expressed and utilized in this study. The residues are numbered according to their position in gp160.

hydrophobic grooves on the surface of the NHR coiled-coil in an antiparallel manner (*8*).

The necessity of SHB for the transition from the prefusion to the postfusion state was demonstrated extensively by mutagenesis (*11, 12*) and by ectodomain derived synthetic peptides that inhibit its formation, resulting in the inhibition of the fusion process (*7, 10, 13*−*16*). On the basis of these findings and on the fact that SHBs are found in many viral proteins, it has been assumed that the SHB is the postfusion thermo-stable conformation of gp41 (*8, 9, 14, 17*), and it serves to bring the viral and cell membranes into close apposition, while the FP and the transmembrane spanning domain are responsible for membrane fusion and pore expansion (*1, 2, 18*). However, other regions were found within gp41 that could be directly involved in membrane destabilization and fusion (*4*, *19*, *20*, *34*, *41*−*44*). Furthermore, recent studies also revealed that a SHB core complex comprised of synthetic peptides is stable in the presence of zwitterionic PC phospholipid membranes that are the major component of the outer surface of cells but are unstable in the presence of negatively charged phosphatidylserine (PS) membranes (*19, 20*). The outer leaflet of cells is composed mainly of zwitterionic phospholipids. Nevertheless, studies on the association of apoptosis (not bystander apoptosis, ref *21*) with the progression of acquired immune deficiency syndrome (AIDS) have revealed that PS, a hallmark of programmed cell death, is expressed at elevated levels in HIV-1-infected T cells or macrophages (*22, 23*). In addition, syncytium formation has been shown to amplify apoptotic signals (*24*).

Despite the enormous studies described above, the influence of the membrane on the structure, core stability, and membrane perturbing activity has not yet been studied using the entire gp41 ectodomain. The poor solubility of gp41 when expressed in *Escherichia coli* has required the use of chimera proteins, deletion mutagenesis, or limited proteolysis to generate soluble gp41 ectodomain constructs (*14, 25*−*27*). These approaches have led to the removal of functional determinants that are located outside SHB domain, such as the FP, the PTD, and the loop, that are directly involved in the lipid mixing event during membrane fusion (*8, 17, 27, 28*).

Here we report on the expression, purification, thermal stability, and characterization in solution and membranes of the entire gp41 ectodomain, as well as its two deletion mutants (Figure 1): (i) the gp41 ectodomain lacking the FP and the polar region (termed extended core/e-core) and (ii) the gp41 ectodomain lacking the PTD, the polar region, and the FP (termed core). The results support the emerging model in which one of the roles of gp41 folding into SHB conformation is to slow down membrane disruption effects induced by early exposed gp41. However, it can further affect membrane morphology once exposed to negatively charged membranes during late stages.

## MATERIALS AND METHODS

*Materials.* LPC and PC (from egg yolk) were obtained from Sigma. LPS and PS (from porcine brain) were obtained from Avanti. *N*-(lissamine rhodamine B sulfonyl) dioleoylphsphatidylethanolamine (Rho-PE) and *N*-(7-nitrobenz-2-oxa-1,3-diazol-4-yl) dioleophosphatidylethanolamine (NBD-PE) were purchased from Molecular Probes (Eugene, OR). All other reagents were of analytical grade.

*HIV-1 gp41 Ectodomain Cloning, Expression, and Purification.* Gp41 from the HIV-1 strain HXB2 was cloned into a pET24d plasmid (*29*) between *Hin*dIII and *Bam*HI sites. For this, the intrinsic *Hin*dIII site was canceled by directed mutagenesis. Also the two cysteines in the loop were mutated to alanines. The sequence of the ectodomain starts from 512 and extends to 684, the sequence of e-core starts from 546 to 684, and the sequence of the core starts from 538 to 666 (Figure 1). Asparagine and glycine were inserted between TrpdelE and gp41 for future nonenzymatic cleavage. The proteins were expressed in BL21 pLys S *E. coli* grown in Luria Broth (LB) supplemented with kanamycin up to an $OD_{600}$ of 0.4. Then 1 mM of IPTG was added to induce expression. The chimeras were located in inclusion bodies and were purified by sonicating the cells and centrifugation at 15 500 rpm at 4 °C for 30 min, following washing the inclusion bodies six times with Lysis buffer (50 mM Tris at pH 7.0, 100 mM NaCl, 5 mM ethylenediaminetetraacetic acid, 0.1 mM phenylmethanesulphonyl fluoride, 0.1% Triton X-100). The purified chimeras were then nonenzymatically cleaved by hydroxylamine between asparagine and glycine (*30*). The products of the reactions were separated by reverse phase high-performance liquid chromatography at 80 °C using a C18 column and a gradient of 25−80% acetonitrile in water during 40 min. The eluted proteins were then dialyzed for 24 h against 50 mM sodium formate buffer (pH 3) at 4 °C using a 3 kDa cutoff dialysis cassette. The dialyzed proteins were concentrated by centricones (Millipore) and verified by mass spectrometry. The construct of the core was treated differently as it was in the soluble fraction of the cell. Cells were lysed in the presence of glacial acetic acid, and the protein was purified as previously described (*31*).

*Preparation of Large Unilamellar Vesicles.* Thin films of PC or PC:PS (3:2) were generated from a solution of the lipids in a 2:1 (v/v) mixture of $CHCl_3$/MeOH that was dried under a stream of nitrogen while rotating. Two populations of films were generated: (1) lipid only mixtures, termed unlabeled, and (2) the same lipid mixture containing 0.6% molar of NBD-PE and Rho-PE each, termed labeled. The films were lyopholized overnight, sealed with argon gas to prevent oxidation, and stored at −20 °C. Before the experiment, the films were suspended in phosphate buffered saline (PBS) buffer −/− (without $Ca^{2+}$ and $Mg^{2+}$) and vortexed for 1.5 min. The lipid suspension underwent five cycles of freezing−thawing and then extrusion through polycarbonate membranes with 1 and 0.1 μm diameter pores to create LUVs as envisioned by negative staining electron microscopy.

*Fluorescence Spectroscopy.* All fluorescence measurements were performed on a SLM-AMINCO Bowman series 2-luminescence spectrometer at room temperature. Typical spectral bandwidths were 8 nm for excitation and 8 nm for emission. The sample was placed in a 5 mm × 5 mm quartz cuvette with constant magnetic stirring. The data were corrected for background intensities and progressive dilution.

*Lipid Mixing Assay.* Lipid mixing of LUVs was measured using a fluorescence-probe dilution assay. LUVs were prepared with PBS, as described above, and then diluted with 50 mM sodium formate buffer at pH 3 to a final concentration of 100 μM in a mixture of unlabeled and labeled films, at a 9:1 ratio. The basal fluorescence level was measured initially for a 400 μL vesicle mixture. Then, proteins dissolved in a maximum volume of 20 μL of sodium formate buffer were added. Fluorescence was monitored for a maximum of 10 min after addition of the protein, to ensure a steady state, as indicated by a plateau. The emission of NBD, the energy donor, was monitored at 530 nm with the excitation set at 467 nm. Fluorescence intensity before protein addition was referred to as 0% lipid mixing. A 100% lipid mixing was normalized according to the signal obtained after addition 0.03% Triton-X-100.

*Preparation of Supported Lipid Bilayers for Atomic Force Microscopy (AFM).* Supported lipid bilayers were prepared using the vesicle fusion method (*32*). Briefly, PC and PC:PS (3:2) LUV suspensions (1 mM, 70 μL) were deposited onto freshly cleaved mica squares (1 $cm^2$) and allowed to adsorb and fuse on the solid surface for 4 h at 25 °C. Samples were then placed in an atomic force microscope.

*AFM Experiments.* Supported bilayers were investigated using a MultiMode atomic force microscope with Nanoscope V controller (Veeco Metrology LLC, Santa Barbara, CA) equipped with a small scanner (E-scanner). AFM images were obtained in semicontact mode in the buffer solution at room temperature (23−25 °C). The long series of images has been taken regularly before protein injection. This was done to verify that the effect of protein interaction with the membrane is not produced by the prolonged scanning itself. Furthermore, before adding the protein solution, the AFM probe was withdrawn on 150−200 nm only to ensure a change tracking at the same area. The scanning has been resumed immediately after protein injection and continued over the same amount of time as the series before the injection. In addition, the "reference point", like single small membrane corrugation, was checked before and after the protein injection where it was possible to verify again that the same area was scanned. The proteins were dissolved in 50 mM sodium format buffer (pH 3). Next, they were injected into the buffer to reach approximately 0.9 μM protein concentration, and images were taken continually every 3−5 min. All images were recorded using oxide-sharpened microfabricated $Si_3N_4$ cantilevers (DNP-S, Veeco Metrology LLC, Santa Barbara, CA) with a spring constant of ∼0.12 N/m (manufacturer specified) and at a scan rate of 1.5−3.5 Hz.

*CD Spectroscopy.* The CD spectra of the proteins were measured in an Aviv 202 spectropolarimeter. The spectra were scanned with a thermostatted quartz optical cell with a path length of 1 mm. Spectra were recorded at 1 nm intervals with an average time of 10 s, at a wavelength range of 260−190 nm. The proteins were scanned at a 5 μM concentration in three different environments: 50 mM sodium formate buffer (pH 3), LPC 1%, and LPC:LPS 1% (3:2). The signals of the buffer, LPC 1%, and LPC:LPS 1% (3:2) before adding the proteins were subtracted from the signals after protein addition. Following spectral acquisition, thermal melts were recorded at 222 nm and were based on the following parameters: temperature range (25−110 °C), temperature step of 3 °C, 10 s averaging time, 2 min incubation prior to each measurement, and 1 min ramp for each 2 °C temperature increase.

*DSC.* DSC was run in a Nano II differential scanning calorimeter (Calorimetry Sciences Corp., Linden, UT). The cell volume was 0.34 mL. The gp41 ectodomain (4.2 mg) was dissolved in 2 mL of 50% acetonitrile/water with 0.1% trifluoroacetic acid and dialyzed in Pierce dialysis cassettes (10kD cutoff) against two changes of 500 mL each of 50 mM formic acid, pH 3 at 4 °C. The final solution concentration was 40 μM protein, as determined by the bicinchoninic acid (BCA) protein assay (Pierce) in triplicate aliquots of 20 μL each. Protein was kept at 4 °C until use. DSC was run from 20 to 125 °C, at 2°/min, against 50 mM formic acid at pH 3. Data were plotted in Origin 5.0 and analyzed with the program DA-2 provided by MicroCal, Inc.

## RESULTS

*Expression and Purification of gp41 Ectodomain, e-Core, and the Core.* We expressed the gp41 ectodomain fused to trpdelE carrier protein in *E. coli*. The trpdelE directs the protein to inclusion bodies, thus surpassing the problem of the nonsolubility of the protein. After purification of the expressed chimera, nonenzymatic cleavage (*30*), purification, and refolding were performed. Both the entire ectodomain and the extended core were isolated using this methodology. Figure 2 shows an example of sodium dodecyl sulfate polyacrylamide gel electrophoresis (SDS-PAGE) of samples taken from three stages in the expression and purification process of the full-length HIV gp41 ectodomain. Note that the purified protein appears in two lanes. Both lanes are the pure protein as verified by mass spectrometry and represent monomer and dimer states. SDS is an acidic detergent which disrupts the isolated SHB core (*8, 19*) and hence prevents the formation of trimers. However, because of the high hydrophobicity of the entire ectodomain, it can dimerize under these conditions similarly to those of membrane proteins. The core alone of gp41 is not toxic to the cells,

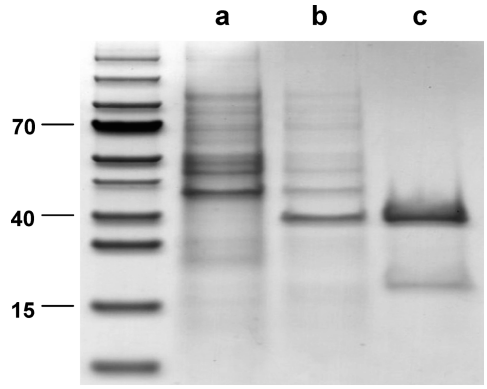


FIGURE 2: SDS-PAGE of samples taken from three stages in the expression and purification process of the HIV gp41 ectodomain. Lane a, uninduced cells; lane b, induced cell by IPTG where the most obvious band represents the ectodomain attached to the trpdelE; lane c, pure gp41 ectodomain obtained by nonenzymatic cleavage and separation in the HPLC. The two bands in c represent monomer and dimer states (see Results section).

and hence it was expressed in *E. coli* as a soluble protein. All experiments were done in an acidic environment, since it has been shown previously that the gp41 ectodomain, containing the core and the loop of HIV-1 (*33*) and simian immunodeficiency virus (SIV) (*26*), and gp41 tend to aggregate at neutral pH, whereas at pH 3 the protein stays in its soluble trimeric state. All three proteins analyzed in this work were treated with proteinase K and revealed a protease resistant core (data not shown), which implies correct folding under the conditions used. In addition, CD analysis showed a high α-helical structure, as described below.

*Lipid Mixing Activity of gp41 Ectodomain and Its Mutants.* We compared the lipid mixing activity of gp41 ectodomain, e-gp41, and the core segment using both zwitterionic (PC) and negatively charged (PC/PS) lipids. PC is the major component of the outer leaflet of uninfected cells, whereas PS, a hallmark of programmed cell death, is expressed at elevated levels in HIV-1-infected T cells or macrophages because of the association of apoptosis with the progression of AIDS (*22, 23*). We used as a reference the fluorescent signal obtained after the addition of 0.03% Triton to the liposome solution. The data, shown in Figure 3 panels a and b, reveal that all three proteins are remarkably active in inducing fusion of negatively charged membranes, while they are practically inert toward zwitterionic membranes. The gp41 is active already at a 0.0005 peptide/lipid molar ratio. For comparison, the most fusogenic domain of gp41 found so far, which comprises the 70-aa of the extracelluar domain of gp41, containing both the FP and the NHR (*34*) or a trimeric HIV-1 FP construct (*18*), is about 10-fold less active under similar conditions, whereas the FP alone is about 100-fold less active (*20, 34*). Note that this pH is lower than that commonly used in fusion assays of HIV-1 derived peptides (pH ≈ 7.0) (*18, 34*). Under low pH, protonation of the carboxyl group in the PS headgroup in PS vesicles results in major changes in the effective shape of PS (*35*). However, fusogenic regions within gp41 such as N-54; ref *20*) preserve their ability to induce fusion of PS/PC vesicles also at pH 3 (data not shown). We also monitored the kinetics of the membrane fusion, and the data are shown in Figure 3c. The data reveal that all three proteins act immediately after their addition to the liposome solution.

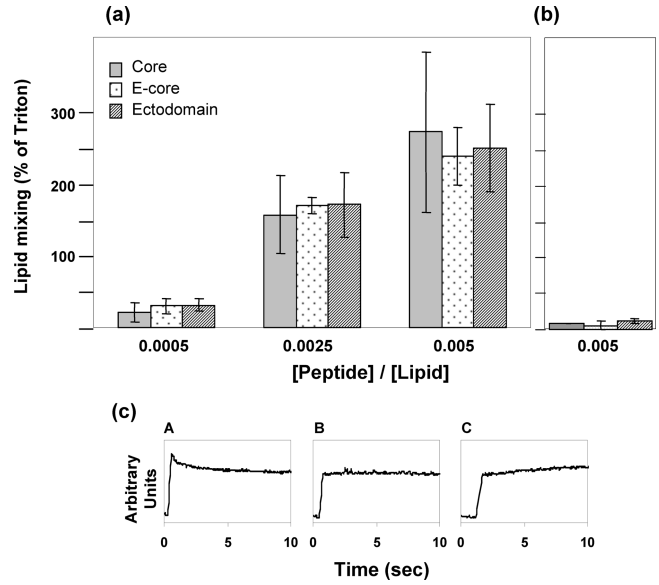


FIGURE 3: Dose-dependent lipid mixing of PC:PS (3:2) LUV (a) and PC LUV (b), induced by the ectodomain, the extended core, and the core. Bars in a and b indicate the standard deviation of experimental measurements. Protein aliquots were added to 100 μM LUV containing 10% prelabeled LUV with 0.6 mol % NBD-PC and Rho-PC in PBS buffer. Fluorescence intensity was measured 5 min after addition of the proteins. The reference was the fluorescent signal obtained after the addition of Triton X-100 to the LUV solution to a final concentration of 0.03%. The results in panel a were plotted as a function of the peptide/lipid molar ratio. The kinetics of the lipid mixing assay (c). The changes in the fluorescence (arbitrary units) plotted vs time (s), after adding a protein (peptide to lipid molar ratio of 0.0025), are shown. The protein's core, the extended core, and the ectodomain are shown in panels A, B, and C.

*Real-Time AFM Exhibits Nanoscale Holes in Negatively Charged Membranes Induced by the gp41 Ectodomain and Its Mutants.* Topographic images obtained for PC and PC:PS (3:2) bilayers in sodium formate buffer (50 mM, pH 3) revealed a single phase, continuous membrane layer, roughly 5 nm deep (data not shown). The ectodomain, the e-core, and the core (∼0.9 μM) were added under the same conditions to the two different types of bilayers. Topographic images of a constant square (1 μm × 1 μm) were taken every 3−5 min. Figure 4 shows three representative pictures of each protein with the two different bilayers. In agreement with the lipid mixing results, all three proteins acted in a similar way: their effect on PC bilayers was insignificant, while on PC:PS they caused a dramatic and equivalent damage to the membrane. The membrane destruction caused by the proteins was gradual; after the first 25 min, the nanoholes depth extended only to the upper layer (∼2 nm), and after 40 min it expanded to the whole bilayer (∼4 nm) (see movie in the Supporting Information).

*Secondary Structures of gp41 Ectodomain and Its Mutants in Solution and Micelles.* CD spectroscopy was used to examine the influence of zwitterionic and negatively charged membrane mimetic environments on the structure of the three proteins. The CD spectrum of each protein was recorded at 25 °C, in 50 mM sodium formate buffer at pH 3 and in two different membrane mimetics, 1% LPC and 1% LPC:LPS (3:2) micelles. The data, shown in Figure 5, clearly demonstrate that the spectra of all proteins examined in buffer and in micelles have double minima at ∼208 and ∼222 nm, characteristic of an α-helical structure. The data reveal the

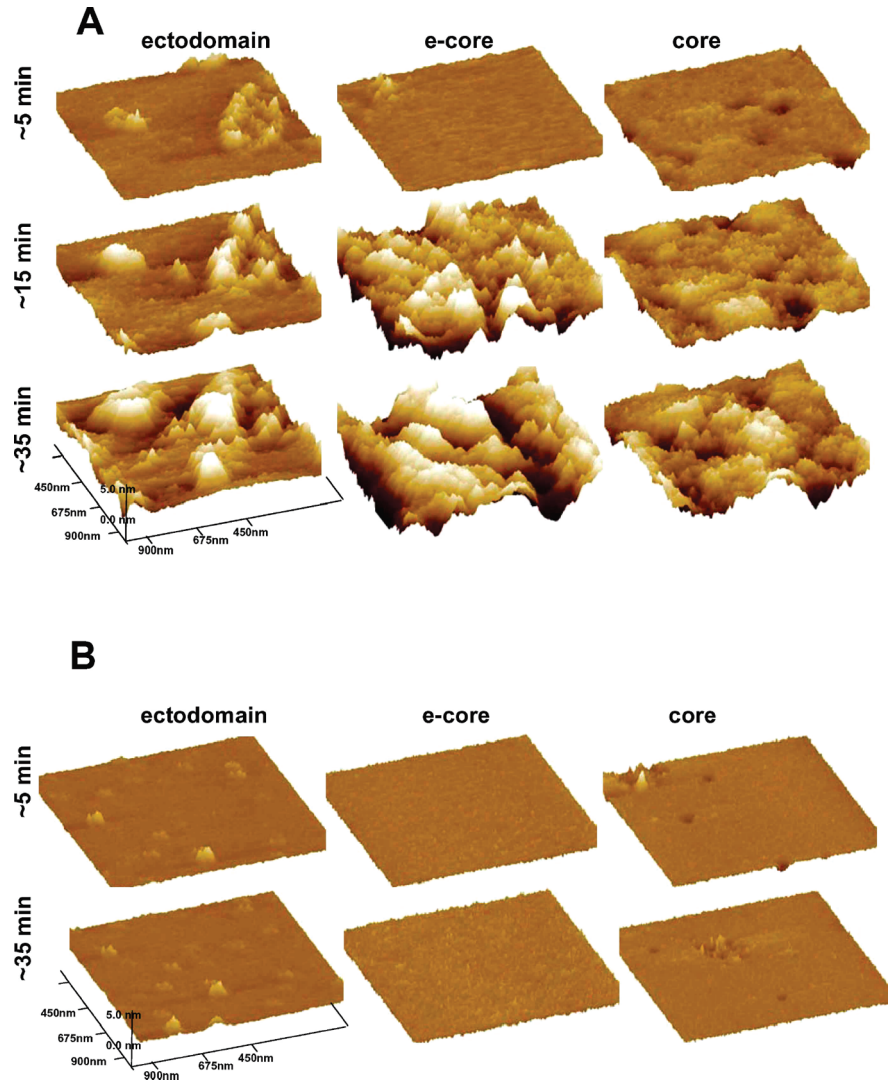


FIGURE 4: Real-time AFM images (1 $\mu$m × 1 $\mu$m; $z$ scale, 5 nm) showing the interaction between PC:PS (3:2) (A) and PC (B) bilayer membranes and the core, the extended core, and the ectodomain. The interactions were imaged in real time, in aqueous buffer with AFM. After protein addition to the bilayer, new topographic images were taken every few minutes.

following order of helicity: core > e-core > ectodomain (Figure 5). This is expected since the core segment is the main contributor of the α-helical structure in the gp41 ectodomain and the fractional helicity of a protein is directly proportional to its mean residue ellipticity at 222 nm. Furthermore, the ratio $\theta_{222}/\theta_{208}$ can be indicative of the extent of coiled-coil in proteins (*36, 37*). Here a reduction in the ratio $\theta_{222}/\theta_{208}$ in micelles compared to buffer suggests less coiled-coil structure in the micelles compared to buffer. The smallest effect is observed with the entire ectodomain in which the contribution of the α-helical structure is the lowest one.

*Thermal Stability of gp41 Ectodomain and Its Mutants in the Absence and Presence of Lipids.* The stability of a protein depends on its tertiary structure. We analyzed the thermal stability of the gp41 ectodomain, e-gp41, and the core protein in membrane mimetic and aqueous environments, by monitoring the melting profile at 222 nm using CD spectroscopy. Figure 6 shows the thermal denaturation profiles of the ectodomain, the e-core, and the core in three different environments: 50 mM sodium formate buffer at pH 3, 1% LPC, and 1% LPC:LPS (3:2). In micelles all three proteins exhibit a similar phenomenon; they all have a gradual linear decrease ($R^2 = 0.99$) in their α-helical structure. In the sodium formate buffer, each protein behaves differently and has a different $T_m$ point. The $T_m$ of the e-core is 70 °C; the $T_m$ of the core could not be precisely defined, though a reduction in its helical structure started to be observed at 100 °C. For the ectodomain, a characteristic $T_m$ curve in the graph is not seen at all, since its $T_m$ might exceed 110 °C, which was the maximum value of the temperature scan. Interestingly, although the proteins exhibit different thermal stability in the sodium formate buffer and in the membrane environment, the final extent of the profile change at 222 nm between 25 and 110 °C in the two types of environments for each protein is similar. These results support the notion that the SHB is less stable in a membrane environment compared to buffer.

*Thermal Stability of the Core in Solution and Micelles Determined by DSC.* We used DSC to determine the thermal stability of the core so as to access higher temperatures and to monitor unfolding processes not involving changes in secondary structure. Experiments were performed both in solution or when the proteins were bound to zwitterionic LPC micelles. Addition of the protein to LPS resulted in the solution acquiring a homogeneous intense turbidity and

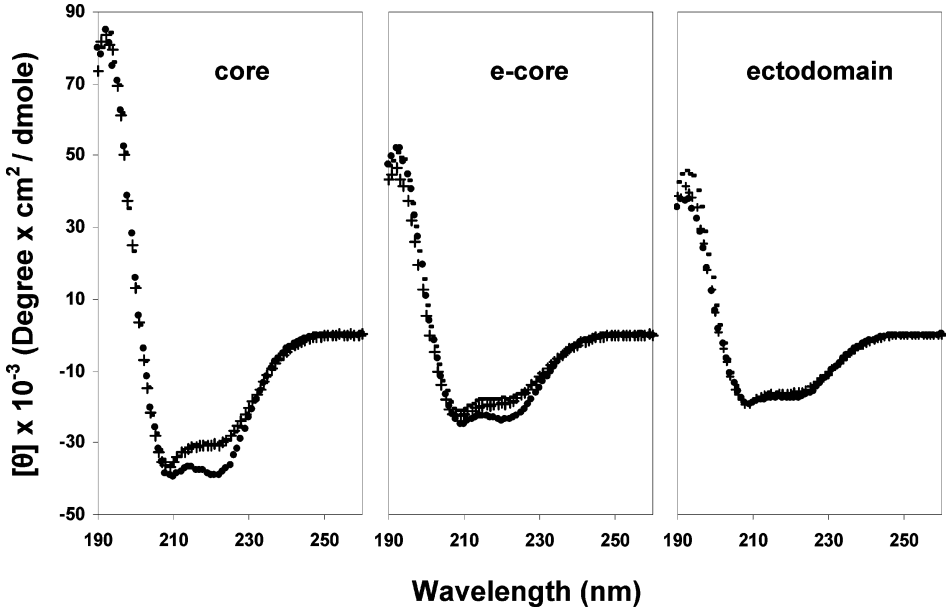


FIGURE 5: CD spectra of the core, the e-core, and the ectodomain were taken at 25 °C. A 5 $\mu$M portion of each protein was added to 50 mM sodium formate buffer (pH 3) [●], LPC 1% in 50 mM sodium formate buffer [−], and LPC:LPS (3:2) 1% in 50 mM sodium formate buffer [+]. The measured ellipticity was converted to molar ellipticity.

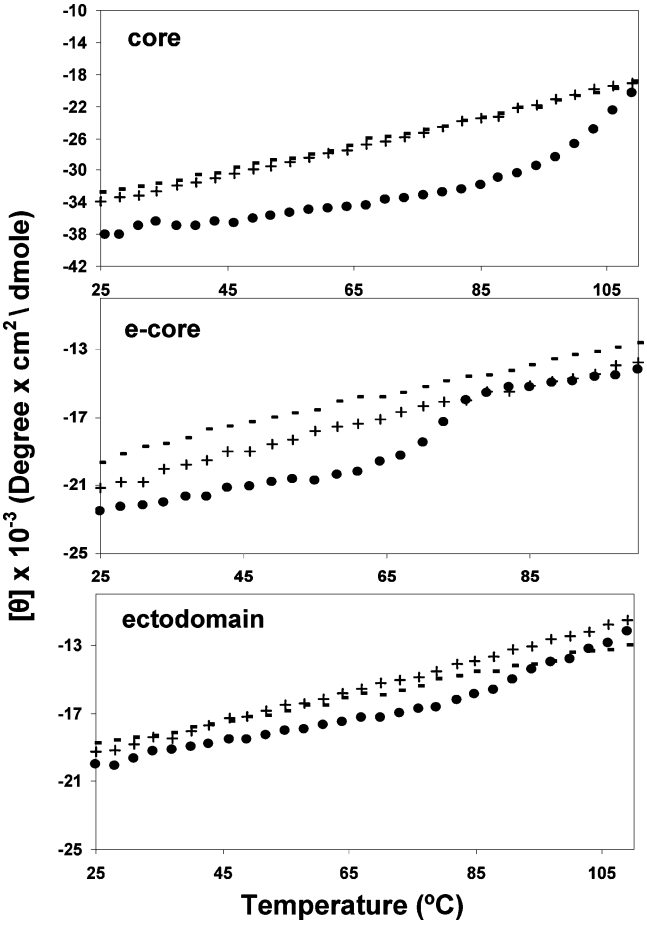


FIGURE 6: Thermal stability of the folded core, the e-core, and the ectodomain as measured by the CD spectra. The curve was recorded at 222 nm after addition of 5 $\mu$M of each protein to 50 mM sodium formate buffer (pH 3) [●], LPC 1% in 50 mM sodium format buffer [−], and LPC:LPS (3:2) 1% in 50 mM sodium formate buffer [+]. The measured ellipticity was converted to molar ellipticity.

therefore was not studied further. In all cases DSC was run from 20 to 125 °C, at a scan rate of 2°/min, in 50 mM sodium formate, pH 3. The results for the protein alone are shown in Figure 7A. A denaturation peak was found in the first heating scan (scan 1) at 104.6 °C, with an enthalpy of 86 kcal/mol of monomer and a van't Hoff enthalpy of 190 kcal/mol (Table 1). This corresponds to a cooperative unit size of two, indicating that the thermal unfolding occurs by the cooperative unfolding of two monomers. The calorimetric enthalpy of unfolding of 86 kcal/mol monomer corresponds to 5.7 cal/g. This value is lower than that of the average soluble protein denaturation at about 100 °C that has an enthalpy of ~10 cal/g (*38*). It is, however, higher than the value for many integral membrane proteins that is about 3 cal/g (see ref *39*). Thus, the value is intermediate between that of a soluble protein and that of an integral membrane protein. Interestingly, it is close to the value of 4.5 cal/g reported for the hemagglutinin fusion protein of the influenza virus (*40*). In the present example of the gp41, the protein is an ectodomain. However, the transmembrane segment represents a small fraction of the total protein. With the gp41 ectodomain, denaturation was partially reversible after heating to 125 °C, showing a peak in the cooling scan (scan 2) at 104 °C with a minor broader component at 93.5 °C. In the second heating scan (scan 3) and second cooling scan (scan 4), both components were still present but with progressively reduced enthalpy. Table 1 shows the thermodynamic parameters of the scans. Overall, the partial reversibility of the renaturation/denaturation process further supports the presence of a stable core of gp41. The DSC data are also in agreement with the data obtained by using CD spectroscopy; that is, the melting of the core in aqueous solution starts at about 100 °C in the CD experiments and is in agreement with the DSC experiments (Figure 7).

For the DSC runs with micelles, the protein was diluted 1:1 with 2 mg/mL LPC in 50 mM formic acid, pH 3, at a lipid/protein molar ratio of 95. The mixture in solution was clear. The DSC was run under the same conditions as in Figure 7. We found only a residual small feature in the range of 100−120 °C in LPC (Figure 7B). The control

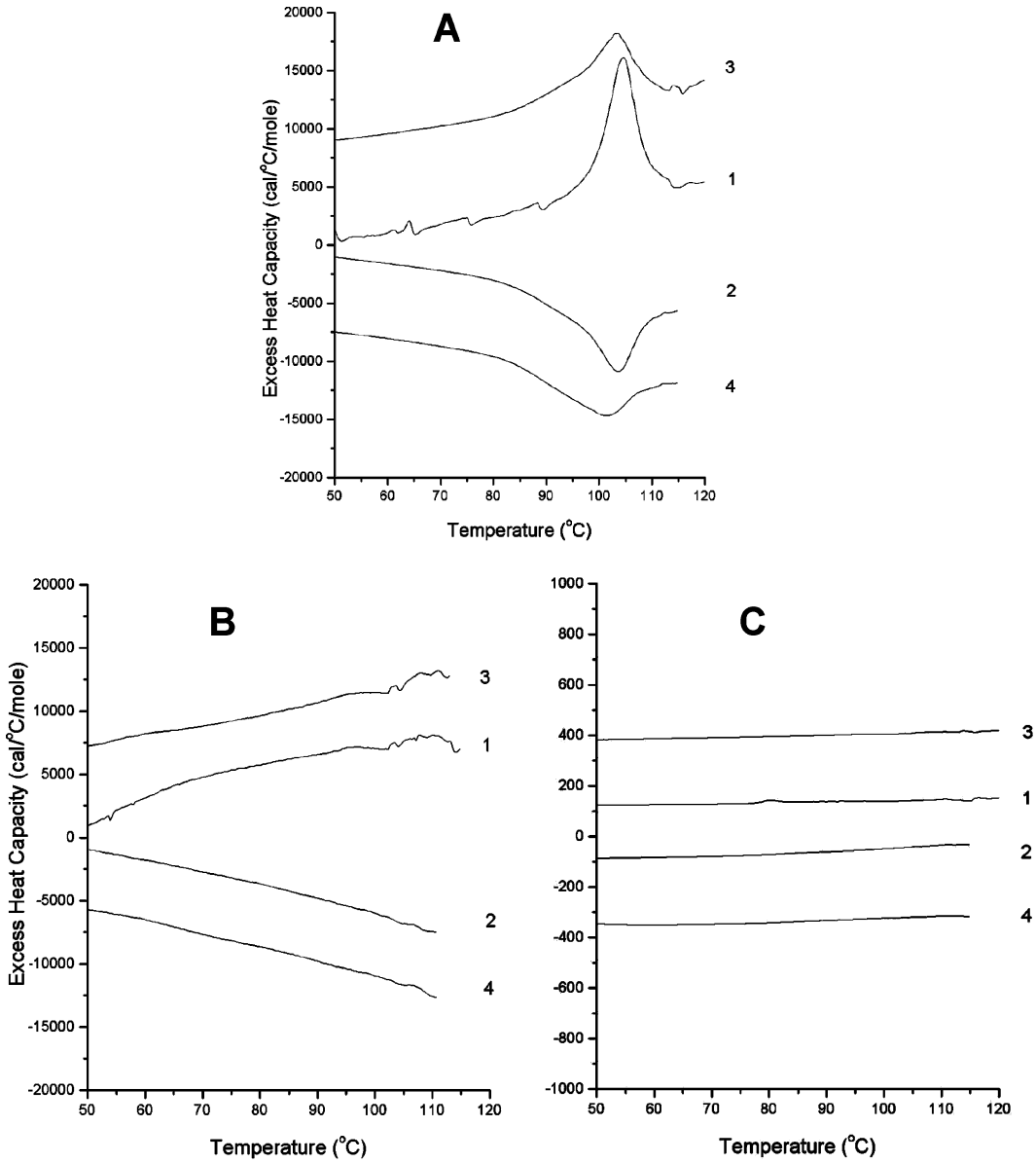


FIGURE 7: (A) Thermal unfolding of the soluble core by DSC. A 0.625 mg/mL portion of the gp41 ectodomain (42 $\mu$M) dialyzed against 50 mM formic acid, pH 3 at 4 °C, was successively scanned by DSC at a scan rate of 2°/min using 50 mM formic acid, pH 3, in the reference cell. Odd-numbered scans are successive heating scans, and even numbers are successive cooling scans. (B) Thermal unfolding of the membrane bound core by DSC. DSC profile of 42 $\mu$M gp41 ectodomain diluted 1:1 with 2 mg/mL LPC in 50 mM formic acid, pH 3. Lipid to protein molar ratio is 95. Scans run at 2°/min against formic acid, pH 3. Odd numbers are successive heatings and even numbers successive coolings. (C) Control with 4 mM LPC with no added protein. Note the 20-fold expansion of the *Y*-axis in comparison with section A.

Table 1: Thermodynamic Parameters for the Denaturation of the Soluble Core Determined from DSC Scans[a]

| scan no. | peak type | $T_D$ (°C) | $\Delta H°$ (kcal/mol monomer) | $\Delta H*$ (kcal/mol) |
|---|---|---|---|---|
| 1 | major | 104.6 | 86 | 190 |
| 2 | major | 104 | 58.5 | 310 |
| 2 | minor | 93.5 | 28 | 210 |
| 3 | major | 103 | 50 | 340 |
| 3 | minor | 93.5 | 24 | 230 |
| 4 | major | 101 | 44 | 250 |
| 4 | minor | 93.5 | 18 | 150 |

[a] $T_D$ = denaturation temperature; $\Delta H°$ = calorimetric enthalpy; $\Delta H*$ = van't Hoff enthalpy related to cooperativity.

with LPC in the absence of protein showed a flat line over the entire range (Figure 7B, note the 20-fold change in scale).

## DISCUSSION

Many studies have been carried out on the interaction between synthetic peptides derived from HIV-gp41 and various model phospholipid membranes. These peptides were shown to induce destabilization of lipid bilayers and fusion of liposomes and cells (*4, 19, 20, 34, 41*−*44*). Here we investigated the interaction between the entire extracellular domain of gp41 with membranes and membrane mimetic micelles. We first expressed and purified the full-length HIV-gp41 ectodomain in a soluble form without addition of a foreign proteinaceous attachment to assist the protein solubility. Importantly, we show that the folded gp41 ectodomain is extremely efficient in inducing lipid mixing of negatively charged membranes, whereas its activity is negligible toward zwitterionic membranes (Figure 3 and Supporting Information). Its activity is about 100-fold higher than that of the FP (*20, 45*). The high lipid mixing

ability of the entire ectodomain compared to its synthetic fragments is probably due to a synergism among all of the active domains. This is demonstrated, for example, by the finding that the FP and NHR regions act synergistically only when linked together but not when mixed as separate peptides (*20, 34*). An interesting observation is that all three proteins showed similar fusogenic activities. This can be explained by the fact that all of the constructs contain regions that have been shown to induce lipid mixing. These include the FP, the NHR, the loop, and the membrane proximal domain (*4, 19, 43, 45, 46*). It has been shown that the core is destabilized in the presence of negatively charged membranes (*19, 20*). Therefore, these membrane active regions should be more exposed to act synergistically to perturb the membrane. In contrast, the core of gp41 remains stable in the presence of zwitterionic membranes, as has been shown previously with synthetic NHR and CHR peptides (*20*), and here with the entire ectodomain, although less compared to buffer (Figure 7). Further support comes from the AFM results, revealing that all three proteins damage the negatively charged membrane bilayer significantly (Figure 4 and Supporting Information). A similar phenomenon was observed with the ectodomain of the influenza hemagglutinin fusion protein which is triggered by low pH to induce damage to bilayers deposited on mica (*47*). Note that the kinetics in the lipid mixing assay is faster than that of the AFM studies. This is because the experiments of membrane fusion were done by mixing together the proteins and vesicles, both in solution, whereas in the AFM experiments the peptides reach the lipid layer by diffusion, which is a slow process.

*Stability of the Proteins.* Our data also reveal that all three proteins exhibit α-helical structures and high thermal stability in an aqueous solution, indicating that all three proteins can form a highly stable SHB in aqueous environment. The core of all three proteins is also substantially stable in a zwitterionic membrane mimetic environment. However, there is a reduction in the secondary structure of the protein as shown by a decrease in the magnitude of the ellipticity, and that unfolding transition is essentially eliminated, as shown by DSC (Figure 7). The latter might indicate that the structural transition is broader and less cooperative because of a transition to a less folded conformation. In addition, there is an overall reduction in the $\theta_{222}/\theta_{208}$ ratio in the lipidic environment which suggests a reduction in the coiled-coil conformation (*36, 37*). Taken together, these data indicate that the membrane mimetic environment drives the proteins into a partially unfolded conformation. Indeed, an X-ray structure of N34(L6)C34 in the presence of SDS revealed that the lower ellipticity in the presence of SDS is due to a partially unfolded region in the molecule (*48*).

Interestingly, no significant difference was observed in the structure of the proteins and their thermal stability in the presence of negatively charged or zwitterionic membrane environments, as revealed by using CD spectroscopy, though in the DSC study (data not shown) a precipitation appears as the proteins interact with LPS. It seems that the strong interaction between the LPS and the core seen in the DSC study and not in the CD spectroscopy is due to higher concentrations of both the proteins and LPS needed for the DSC experiments.

*Role of the Hairpin in Membrane Fusion.* Identification of the sequential events that take place from the prefusion to the postfusion step have been brought to the front of HIV fusion research since the crystal structure of the gp41 core was resolved (*8*). When gp41 is released from its metastable constrains, the N-terminal FP is thought to be inserted into the target membrane, and gp41 adopts an extended conformation (prefusion intermediate) (*49, 50*). The transition from the prefusion step to the hairpin (postfusion step) structure brings the two membranes into close proximity, driving fusion and stabilizing fusion pores (*50*). The insertion of the FP into the target zwitterionic membrane causes membrane destabilization though this destabilization appears to also be a result of the interaction of additional segments of gp41 with the membrane (*3, 4, 8, 13*). These interactions provide a way to lower the barrier for fusion to take place, which correlates with the ability of the prefusion intermediate of gp41 to direct membrane fusion through the stage of pore formation (*50*). The latter is supported by the findings that the exposed N-70 trimer (composed of the FP and the NHR) is highly fusogenic toward zwitterionic membranes which compose the outer leaflet of the normal cell (*34*). In contrast, as seen in this study, constructs that form stable cores are nonfusogenic to zwitterionic membranes and probably ablate fusogenic function of the extended conformation toward zwitterionic membranes. This correlates with a viral fusion role for the hairpins that involves stabilization of fused bilayer structure (*50*).

Accumulating evidence suggests that most of gp41 segments and also gp41 as a whole, as demonstrated in this study, can interact with negatively charged phospholipids (*20, 43, 44*). Although the outer leaflet of cells is composed mainly of zwitterionic phospholipids, studies on the association of apoptosis (not bystander apoptosis (*21*)) with the progression of AIDS have revealed that PS, a hallmark of programmed cell death, is expressed at elevated levels in HIV-1-infected T cells or macrophages (*22, 23*). In addition, syncytium formation has been shown to amplify apoptotic signals (*24*).

Overall, the results support the emerging model in which one of the roles of gp41 folding into SHB conformation is to slow down membrane disruption effects induced by early exposed gp41. However, it can further affect membrane morphology once exposed to negatively charged membranes during late stages. The ability to work with the entire soluble gp41 ectodomain should facilitate future investigations of the fusion process induced by HIV.

## ACKNOWLEDGMENT

Y.S. is the incumbent of the Harold S. and Harriet B. Brady Professorial Chair in Cancer Research.

## SUPPORTING INFORMATION AVAILABLE

Membrane bilayer activity in movie format. This material is available free of charge via the Internet at http://pubs.acs.org.

## REFERENCES

1. White, J. M., Delos, S. E., Brecher, M., and Schornberg, K. (2008) Structures and mechanisms of viral membrane fusion proteins: multiple variations on a common theme. *Crit. Rev. Biochem. Mol. Biol. 43*, 189–219.
2. Chan, D. C., and Kim, P. S. (1998) HIV entry and its inhibition. *Cell (Cambridge, MA, U.S.) 93*, 681–684.

3. Rabenstein, M., and Shin, Y. K. (1995) A peptide from the heptad repeat of human immunodeficiency virus gp41 shows both membrane binding and coiled-coil formation. *Biochemistry 34*, 13390–13397.
4. Suarez, T., Gallaher, W. R., Agirre, A., Goni, F. M., and Nieva, J. L. (2000) Membrane interface-interacting sequences within the ectodomain of the human immunodeficiency virus typeb 1 envelope glycoprotein: putative role during viral fusion. *J. Virol. 74*, 8038–8047.
5. Berger, E. A., Murphy, P. M., and Farber, J. M. (1999) Chemokine receptors as HIV-1 coreceptors: roles in viral entry, tropism, and disease. *Annu. Rev. Immunol. 17*, 657–700.
6. Kowalski, M., Potz, J., Basiripour, L., Dorfman, T., Goh, W. C., Terwilliger, E., Dayton, A., Rosen, C., Haseltine, W., and Sodroski, J. (1987) Functional regions of the envelope glycoprotein of human immunodeficiency virus type 1. *Science 237*, 1351–1355.
7. Eckert, D. M., and Kim, P. S. (2001) Mechanisms of viral membrane fusion and its inhibition. *Annu. Rev. Biochem. 70*, 777–810.
8. Chan, D. C., Fass, D., Berger, J. M., and Kim, P. S. (1997) Core structure of gp41 from the HIV envelope glycoprotein. *Cell (Cambridge, MA, U.S.) 89*, 263–273.
9. Furuta, R. A., Wild, C. T., Weng, Y., and Weiss, C. D. (1998) Capture of an early fusion-active conformation of HIV-1 gp41. *Nat. Struct. Biol. 5*, 276–279.
10. Munoz-Barroso, I., Durell, S., Sakaguchi, K., Appella, E., and Blumenthal, R. (1998) Dilation of the human immunodeficiency virus-1 envelope glycoprotein fusion pore revealed by the inhibitory action of a synthetic peptide from gp41. *J. Cell Biol. 140*, 315–323.
11. Lu, M., Stoller, M. O., Wang, S., Liu, J., Fagan, M. B., and Nunberg, J. H. (2001) Structural and functional analysis of interhelical interactions in the human immunodeficiency virus type 1 gp41 envelope glycoprotein by alanine-scanning mutagenesis. *J. Virol. 75*, 11146–11156.
12. He, Y., Liu, S., Jing, W., Lu, H., Cai, D., Chin, D. J., Debnath, A. K., Kirchhoff, F., and Jiang, S. (2007) Conserved residue Lys574 in the cavity of HIV-1 Gp41 coiled-coil domain is critical for six-helix bundle stability and virus entry. *J. Biol. Chem. 282*, 25631–25639.
13. Jiang, S., Lin, K., Strick, N., and Neurath, A. R. (1993) HIV-1 inhibition by a peptide. *Nature 365*, 113.
14. Lu, M., Blacklow, S. C., and Kim, P. S. (1995) A trimeric structural domain of the HIV-1 transmembrane glycoprotein. *Nat. Struct. Biol. 2*, 1075–1082.
15. Wexler-Cohen, Y., Johnson, B. T., Puri, A., Blumenthal, R., and Shai, Y. (2006) Structurally altered peptides reveal an important role for N-terminal heptad repeat binding and stability in the inhibitory action of HIV-1 peptide DP178. *J. Biol. Chem. 281*, 9005–9010.
16. Wexler-Cohen, Y., and Shai, Y. (2007) Demonstrating the C-terminal boundary of the HIV 1 fusion conformation in a dynamic ongoing fusion process and implication for fusion inhibition. *FASEB J. 21*, 3677–3684.
17. Tan, K., Liu, J., Wang, J., Shen, S., and Lu, M. (1997) Atomic structure of a thermostable subdomain of HIV-1 gp41. *Proc. Natl. Acad. Sci U.S.A. 94*, 12303–12308.
18. Yang, R., Prorok, M., Castellino, F. J., and Weliky, D. P. (2004) A trimeric HIV-1 fusion peptide construct which does not self-associate in aqueous solution and which has 15-fold higher membrane fusion rate. *J. Am. Chem. Soc. 126*, 14722–14723.
19. Kliger, Y., Peisajovich, S. G., Blumenthal, R., and Shai, Y. (2000) Membrane-induced conformational change during the activation of HIV-1 gp41. *J. Mol. Biol. 301*, 905–914.
20. Korazim, O., Sackett, K., and Shai, Y. (2006) Functional and structural characterization of HIV-1 gp41 ectodomain regions in phospholipid membranes suggests that the fusion-active conformation is extended. *J. Mol. Biol. 364*, 1103–1117.
21. Garg, H., and Blumenthal, R. (2008) Role of HIV Gp41 mediated fusion/hemifusion in bystander apoptosis. *Cell. Mol. Life Sci. 65*, 3134–3144.
22. Callahan, M. K., Popernack, P. M., Tsutsui, S., Truong, L., Schlegel, R. A., and Henderson, A. J. (2003) Phosphatidylserine on HIV envelope is a cofactor for infection of monocytic cells. *J. Immunol. 170*, 4840–4845.
23. Ma, G., Greenwell-Wild, T., Lei, K., Jin, W., Swisher, J., Hardegen, N., Wild, C. T., and Wahl, S. M. (2004) Secretory leukocyte protease inhibitor binds to annexin II, a cofactor for macrophage HIV-1 infection. *J. Exp. Med. 200*, 1337–1346.
24. Scheller, C., and Jassoy, C. (2001) Syncytium formation amplifies apoptotic signals: a new view on apoptosis in HIV infection in vitro. *Virology 282*, 48–55.
25. Lay, C. S., Wilson, K. A., Kobe, B., Kemp, B. E., Drummer, H. E., and Poumbourios, P. (2004) Expression and biochemical analysis of the entire HIV-2 gp41 ectodomain: determinants of stability map to N- and C-terminal sequences outside the 6-helix bundle core. *FEBS Lett. 567*, 183–188.
26. Peisajovich, S. G., Blank, L., Epand, R. F., Epand, R. M., and Shai, Y. (2003) On the interaction between gp41 and membranes: the immunodominant loop stabilizes gp41 helical hairpin conformation. *J. Mol. Biol. 326*, 1489–1501.
27. Krell, T., Greco, F., Engel, O., Dubayle, J., Kennel, A., Charloteaux, B., Brasseur, R., Chevalier, M., Sodoyer, R., and El Habib, R. (2004) HIV-1 gp41 and gp160 are hyperthermostable proteins in a mesophilic environment. Characterization of gp41 mutants. *Eur. J. Biochem. 271*, 1566–1579.
28. Caffrey, M., Cai, M., Kaufman, J., Stahl, S. J., Wingfield, P. T., Covell, D. G., Gronenborn, A. M., and Clore, G. M. (1998) Three-dimensional solution structure of the 44 kDa ectodomain of SIV gp41. *EMBO J. 17*, 4572–4584.
29. Biron, Z., Khare, S., Quadt, S. R., Hayek, Y., Naider, F., and Anglister, J. (2005) The 2F5 epitope is helical in the HIV-1 entry inhibitor T-20. *Biochemistry 44*, 13602–13611.
30. Bornstein, P., and Balian, G. (1977) Cleavage at Asn-Gly bonds with hydroxylamine. *Methods Enzymol. 47*, 132–145.
31. Fass, D., and Kim, P. S. (1995) Dissection of a retrovirus envelope protein reveals structural similarity to influenza hemagglutinin. *Curr. Biol. 5*, 1377–1383.
32. Yang, T., Simanek, E. E., and Cremer, P. (2000) Creating addressable aqueous microcompartments above solid supported phospholipid bilayers using lithographically patterned poly(dimethylsiloxane) molds. *Anal. Chem. 72*, 2587–2589.
33. Wingfield, P. T., Stahl, S. J., Kaufman, J., Zlotnick, A., Hyde, C. C., Gronenborn, A. M., and Clore, G. M. (1997) The extracellular domain of immunodeficiency virus gp41 protein: expression in Escherichia coli, purification, and crystallization. *Protein Sci. 6*, 1653–1660.
34. Sackett, K., and Shai, Y. (2002) The HIV-1 gp41 N-terminal heptad repeat plays an essential role in membrane fusion. *Biochemistry 41*, 4678–4685.
35. Fuller, N., Benatti, C. R., and Rand, R. P. (2003) Curvature and bending constants for phosphatidylserine-containing membranes. *Biophys. J. 85*, 1667–1674.
36. Meng, F. G., Zeng, X., Hong, Y. K., and Zhou, H. M. (2001) Dissociation and unfolding of GCN4 leucine zipper in the presence of sodium dodecyl sulfate. *Biochimie 83*, 953–956.
37. Zhou, N. E., Kay, C. M., and Hodges, R. S. (1992) Synthetic model proteins. Positional effects of interchain hydrophobic interactions on stability of two-stranded α-helical coiled-coils. *J. Biol. Chem. 267*, 2664–2670.
38. Makhatadze, G. I., and Privalov, P. L. (1995) in *Advances in Protein Chemistry* (Anfinsen, C. B., Ed.) Academic Press, New York.
39. Epand, R. F., Epand, R. M., and Jung, C. Y. (1999) Glucose-induced thermal stabilization of the native conformation of GLUT 1. *Biochemistry 38*, 454–458.
40. Epand, R. F., and Epand, R. M. (2003) Irreversible unfolding of the neutral pH form of influenza hemagglutinin demonstrates that it is not in a metastable state. *Biochemistry 42*, 5052–5057.
41. Munoz-Barroso, I., Salzwedel, K., Hunter, E., and Blumenthal, R. (1999) Role of the membrane-proximal domain in the initial stages of human immunodeficiency virus type 1 envelope glycoprotein-mediated membrane fusion. *J. Virol. 73*, 6089–6092.
42. Wexler-Cohen, Y., Sackett, K., and Shai, Y. (2005) The role of the N-terminal heptad repeat of HIV-1 in the actual lipid mixing step as revealed by its substitution with distant coiled coils. *Biochemistry 44*, 5853–5861.
43. Pascual, R., Contreras, M., Fedorov, A., Prieto, M., and Villalain, J. (2005) Interaction of a peptide derived from the N-heptad repeat region of gp41 Env ectodomain with model membranes. Modulation of phospholipid phase behavior. *Biochemistry 44*, 14275–14288.
44. Moreno, M. R., Giudici, M., and Villalain, J. (2006) The membranotropic regions of the endo and ecto domains of HIV gp41 envelope glycoprotein. *Biochim. Biophys. Acta 1758*, 111–123.
45. Nieva, J. L., Nir, S., Muga, A., Goni, F. M., and Wilschut, J. (1994) Interaction of the HIV-1 fusion peptide with phospholipid vesicles:

different structural requirements for fusion and leakage. *Biochemistry 33*, 3201–3209.
46. Tamm, L. K., Crane, J., and Kiessling, V. (2003) Membrane fusion: a structural perspective on the interplay of lipids and proteins. *Curr. Opin. Struct. Biol. 13*, 453–466.
47. Epand, R. F., Yip, C. M., Chernomordik, L. V., LeDuc, D. L., Shin, Y. K., and Epand, R. M. (2001) Self-assembly of influenza hemagglutinin: studies of ectodomain aggregation by in situ atomic force microscopy. *Biochim. Biophys. Acta 1513*, 167–175.
48. Shu, W., Ji, H., and Lu, M. (2000) Interactions between HIV-1 gp41 core and detergents and their implications for membrane fusion. *J. Biol. Chem. 275*, 1839–1845.
49. Dimitrov, A. S., Xiao, X., Dimitrov, D. S., and Blumenthal, R. (2001) Early intermediates in HIV-1 envelope glycoprotein-mediated fusion triggered by CD4 and co-receptor complexes. *J. Biol. Chem. 276*, 30335–30341.
50. Markosyan, R. M., Cohen, F. S., and Melikyan, G. B. (2003) HIV-1 envelope proteins complete their folding into six-helix bundles immediately after fusion pore formation. *Mol. Biol. Cell 14*, 926–938.

BI802243J